Journal of Electrical and Electronic Engineering
2022; 10(6): 215-222
http://www.sciencepublishinggroup.com/j/jeee
doi: 10.11648/j.jeee.20221006.11
ISSN: 2329-1613 (Print); ISSN: 2329-1605 (Online)

High-Power Laser Beam Propagation in Slightly Wet Atmosphere

Yoshito Shuto

Ofra Project, Iruma City, Japan

Email address:
ofra@tuba.ocn.ne.jp

To cite this article:
Yoshito Shuto. High-Power Laser Beam Propagation in Slightly Wet Atmosphere. *Journal of Electrical and Electronic Engineering*. Vol. 10, No. 6, 2022, pp. 215-222. doi: 10.11648/j.jeee.20221006.11

Received: October 26, 2022; **Accepted**: November 9, 2022; **Published**: November 14, 2022

Abstract: The use of high-power lasers in the industry has been rapidly advanced by incorporating flexible-fiber-based beam delivery. In order to deliver high-power laser beam to a distant place, the laser beam must propagate through the atmosphere. When the laser beam propagates through a medium, a fraction of the laser energy is absorbed by the medium. This absorbed power heats the medium and alters the index of refraction of the path, and leads to a distortion of the beam itself. This phenomenon is called thermal blooming. Thermal blooming at λ_0 = 1.08 μm is caused by the absorption of water vapor. In this article, high-power laser beam propagation in a slightly wet atmosphere at λ_0 = 1.08 μm was theoretically investigated. At First, the absorption coefficient (α) of air at 10% relative humidity was estimated. Then, simulation of thermal blooming of Gaussian laser beam with an initial power of 1 kW and a radius of 5 mm was conducted using this α. Under the condition of no wind, the beam intensity decreases rapidly with increasing length z. At z = 16 m, the intensity of laser beam became 1/5 of the initial intensity at z = 0 m. When laser beam propagated in the moist air with transverse air flow, thermal distortion of the beam was not symmetrical around the z axis because of the asymmetry introduced by the one-dimensional wind velocity v. Under the condition of calm uniform wind with v = 0.05 m/s, laser beams propagated only 25 to 30 m at most without damaging the initial beam shape. On the other hand, the beams propagated 65 to 70 m at most without beam-shape deformation under the condition of light uniform wind with v = 0.5 m/s.

Keywords: Laser Beam Propagation, Moist Atmosphere, Thermal Blooming

1. Introduction

The use of high-power lasers in the industry has been rapidly advanced by incorporating flexible-fiber-based beam delivery. The output power from the ytterbium (Yb)-doped fiber lasers has abruptly increased over the past decade [1-6]. A high output power of > 200 W in the continuous-wave (CW) laser operation at the wavelength (λ_0) of 1.08 μm using cladding-pumped Yb-doped silica fibers has been reported [7-29]. High-power laser beams can be transported through short-length delivery fibers [19, 21, 25, 30]. The hollow-core photonic crystal fibers and holey fibers are now implemented as a tool of laser beam delivery in place of traditional optical fibers [31-38].

However, in order to deliver high-power laser beam to a distant place, the laser beam must propagate through the atmosphere. When the laser beam propagates through a medium, a fraction of the laser energy is absorbed by the medium. This absorbed power heats the medium and alters the index of refraction of the path, and leads to a distortion of the beam itself. This phenomenon is called "thermal blooming" [39]. The thermal blooming is particularly noticeable when the CO_2 laser beam propagates through the air at λ_0 = 10.6 μm, and many research institutes have reported on this phenomenon experimentally and theoretically [39-53].

The atmospheric absorption dependence on laser wavelength is very important. In the atmospheric absorption at λ_0 = 1.08 μm, the dominant absorber is water vapor. In previous studies, thermal blooming effect was often neglected because the fiber laser wavelength, λ_0 = 1.08 μm, is near a water vapor transmission window, λ_0 = 1.045 μm [54, 55]. This is true when the laser beams propagate in dry air in areas of low humidity.

However, when propagating laser beams in a humid place like Japan, the laser beam is affected by water absorption. As a result, it is conceivable that the thermal blooming

appears when the laser beams propagate through a moist atmosphere.

In this article, we investigated high-power laser beam propagation in a slightly wet atmosphere at $\lambda_0 = 1.08$ μm.

2. Absorption Coefficient of Water Vapor

The near infrared absorption spectrum of liquid water at 293 K was reported by Curcio and Petty [56].

According to their report, an absorption coefficient α_w of liquid water at $\lambda_0 = 1.08$ μm is 11.31 m^{-1}.

The saturated vapor pressure e_s (Pa) of moist air at temperature T (K) is given by Tetens' equation [57]

$$e_s = 6110 \exp\left[\frac{17.2694(T-273.15)}{T-35.85}\right] \quad (1)$$

By using Eq. (1), the e_s value at $T = 300$ K was estimated to be about 3.535×10^3 Pa. This is the water vapor pressure at 100% relative humidity.

If the saturated water vapor pressure e_s is known, the water vapor density ρ_v (kg m^{-3}) at temperature T and relative humidity h is given by the following equation

$$\rho_v = 0.00217 \frac{he_s}{T} \quad (2)$$

When relative humidity h is 10%, the ρ_v value at $T = 300$ K was estimated to be about 2.557×10^{-3} kg m^{-3} by using Eq. (2).

By comparing this water vapor density with the density ρ (= 996.62 kg m^{-3} [58]) of the saturated water at 300 K, the water content c_w per 1 m^3 of air at 10% relative humidity is given by the following equation

$$c_w = \frac{\rho_v}{\rho} = \frac{0.002557}{996.62} \approx 2.565 \times 10^{-6} \quad (3)$$

By using c_w and α_w, the absorption coefficient α_v of air at 10% relative humidity is given by

$$\alpha_v = c_w \cdot \alpha_w \quad (4)$$

By using Eq. (4), the α_v of air at 10% relative humidity was estimated to be 2.90×10^{-5} m^{-1} at $\lambda_0 = 1.08$ μm.

This α_v value was used in the following calculation as the absorption coefficient α of slightly wet atmosphere.

3. Simulation of Thermal Blooming of Gaussian Laser Beams

Two propagation patterns of the Gaussian laser beams in slightly wet atmosphere were considered in the calculation, as shown in Figure 1.

In pattern (a), there is no relative motion (no wind) between the laser beam and the moist air. Laser beam propagates along the z direction.

On the other hand, in pattern (b), the laser beam propagates in the moist air with transverse air flow. For the sake of analysis, we assumed that there is a uniform wind with the velocity v in the x direction.

In the following subsection, we described the calculation results of Gaussian laser beam propagation in a slightly wet atmosphere with no wind at $\lambda_0 = 1.08$ μm.

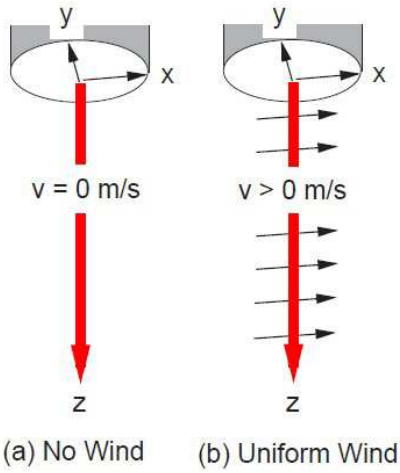

Figure 1. *Laser beam propagation patterns in slightly wet atmosphere.*

3.1. Laser Beam Propagation with No Wind

The intensity of an initially collimated Gaussian laser beam propagating through the slightly wet atmosphere at a point z away from the output end ($z = 0$) is given by

$$I(x, y, z) = I(x, y, 0)e^{-\alpha z} \equiv I_u e^{-\alpha z} \quad (5)$$

This equation does not take into consideration that the thermal distortion of laser beams arises because the absorbed laser power in the atmosphere changes its index of refraction and therefore changes the beam intensity itself.

Taking into account this problem, the steady state solution for the initially Gaussian laser beam was derived as follows: [39, 41]

$$I(x, y, z) = I_u e^{-\alpha z} \times \exp\left\{\frac{\left(\frac{\partial n}{\partial T}\right)P}{\lambda n \pi \omega^2}\left[z + \frac{e^{-\alpha z}-1}{\alpha}\right] e^{-\frac{x^2+y^2}{\omega^2}}\right\} \quad (6)$$

where $\partial n/\partial T$, λ (= 0.02614 W m^{-1} K^{-1} [58]), and n (= 1.000274) are the thermal coefficient of the refractive index, thermal conductivity, and refractive index of the slightly wet atmosphere at 300 K and $\lambda_0 = 1.08$ μm, respectively. P and ω are the initial power and beam radius of the Gaussian laser beam.

$\partial n/\partial T$ is approximately given by the following equation:

$$\frac{\partial n}{\partial T} \cong \frac{\beta(n-1)}{1+\beta(T-273.15)} \quad (7)$$

where β (= 0.003672 [59]) is the body expansion coefficient of air at 1 atm. $\partial n/\partial T$ at $T = 300$ K and $\lambda_0 = 1.08$ μm was estimated to be about -0.92×10^{-6} K^{-1} using Eq. (7).

The intensity distributions of laser beam at $z = 0$, 8, and 16 m were calculated using Eq. (6) when $P = 1$ kW, ω = 5 mm, 10% relative humidity, and $\lambda_0 = 1.08$ μm. The calculated results are shown in Figures 2-4.

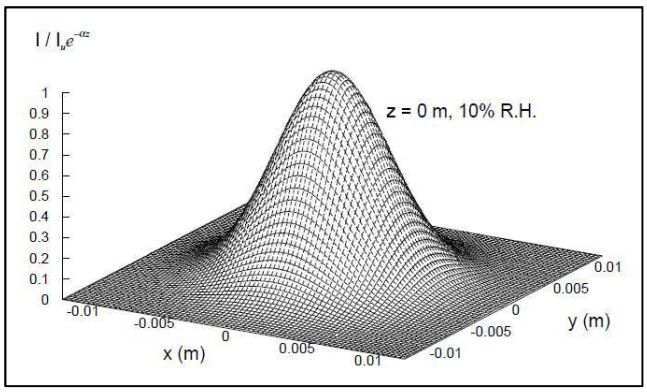

Figure 2. *Normalized intensity distribution of laser beam at z = 0 m. 10% relative humidity.*

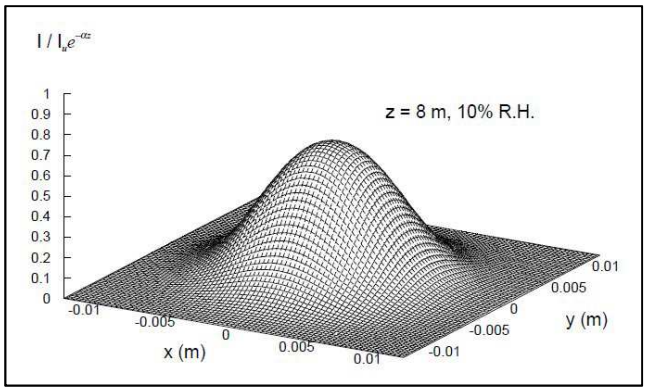

Figure 3. *Normalized intensity distribution of laser beam at z = 8 m. 10% relative humidity.*

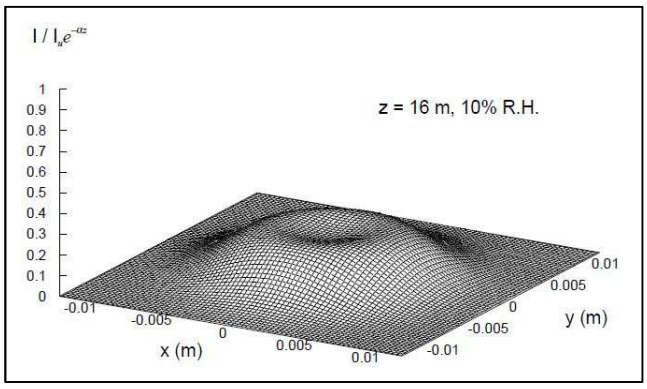

Figure 4. *Normalized intensity distribution of laser beam at z = 16 m. 10% relative humidity.*

In these figures, the intensity I (x, y, z) was normalized by dividing by $I_u e^{-\alpha z}$.

As shown Figures 2-4, the beam intensity decreases rapidly with increasing z. At z = 16 m, the intensity of laser beam became 1/5 of the initial intensity at z = 0 m.

When $\alpha z << 1$, Eq. (6) can be rewritten as [39]

$$\frac{I(x,y,z)}{I_u e^{-\alpha z}} \approx \exp\left[D_c e^{-\frac{x^2+y^2}{\omega^2}}\right] \tag{8}$$

where

$$D_c = \frac{\left(\frac{\partial n}{\partial T}\right) P \alpha z^2}{2\lambda n \pi \omega^2} \tag{9}$$

Since $\partial n / \partial T$ takes a negative value, D_c will take a large negative value as z increases. As a result, the normalized intensity decreases sharply as z increases, as shown in Figures 2-4.

3.2. Laser Beam Propagation with Calm Uniform Wind

When an initially collimated Gaussian laser beam propagates in the moist air with transverse air flow, thermal distortion of the beam is not symmetrical around the z axis because of the asymmetry introduced by the one-dimensional wind velocity.

For the sake of analysis, we assumed that there is a uniform wind with the velocity v in the x direction.

Taking into account this problem, the steady state solution for the initially Gaussian laser beam was derived by Gebhardt and Smith [45]. The solution is as follows:

$$\frac{I(x,y,z)}{I_u e^{-\alpha z}} = \exp\left\{N\left[2\left(\frac{x}{\omega}\right)e^{-\frac{x^2+y^2}{\omega^2}} + \frac{\sqrt{\pi}}{2}e^{-\frac{y^2}{\omega^2}}\left(1-4\frac{y^2}{\omega^2}\right)\left(1+erf\left(\frac{x}{\omega}\right)\right)\right]\right\} \tag{10}$$

where

$$N = \frac{2\left(\frac{\partial n}{\partial T}\right)P}{\rho C_p n v \pi \omega^3}\left[z + \frac{e^{-\alpha z}-1}{\alpha}\right] \tag{11}$$

Here ρ (= 1176.3 kg m^{-3} [58]) and C_p (= 1007 J kg^{-1} K^{-1} [58]) are the density and specific heat of the slightly wet atmosphere at 300 K, respectively. *erf* (x) is the error function with respect to x.

The intensity distributions of laser beam at z = 0, 10, 20, and 30 m were calculated using Eq. (10) when v = 0.05 m/s, P = 1 kW, ω = 5 mm, 10% relative humidity, and λ_0 = 1.08 μm. The calculated results are shown in Figures 5-8. In these figures, the normalized intensity distributions are shown by contour lines with intervals of 0.1.

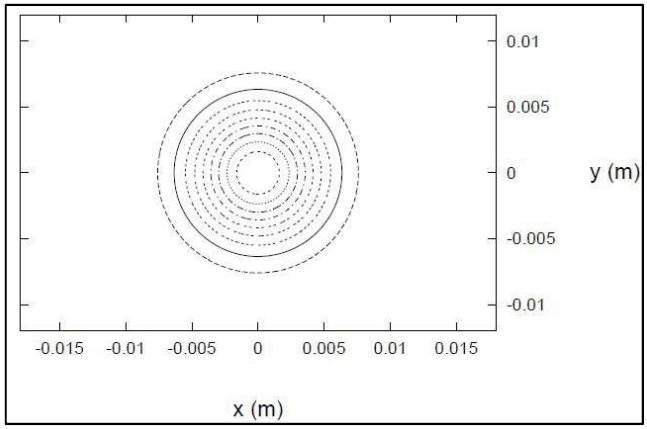

Figure 5. *Normalized intensity distribution of laser beam at z = 0 m with v = 0.05 m/s and 10% relative humidity. Intervals of contour lines are 0.1.*

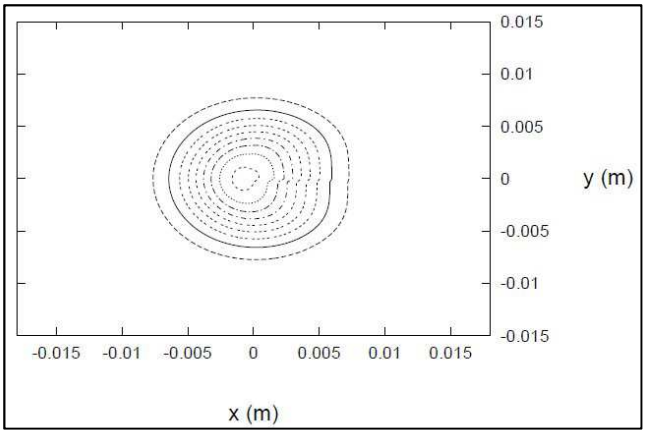

Figure 6. *Normalized intensity distribution of laser beam at z = 10 m with v = 0.05 m/s and 10% relative humidity. Intervals of contour lines are 0.1.*

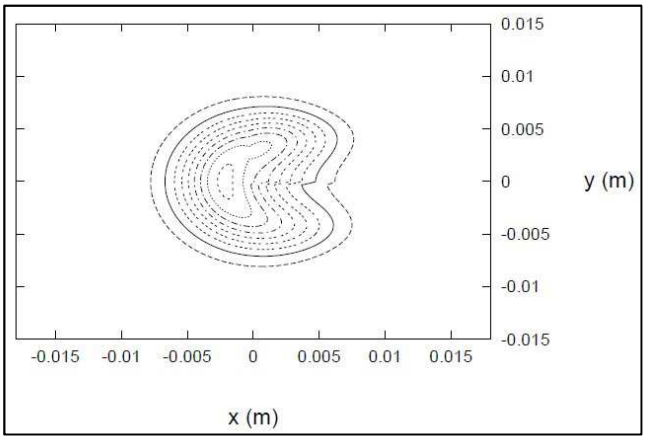

Figure 7. *Normalized intensity distribution of laser beam at z = 20 m with v = 0.05 m/s and 10% relative humidity. Intervals of contour lines are 0.1.*

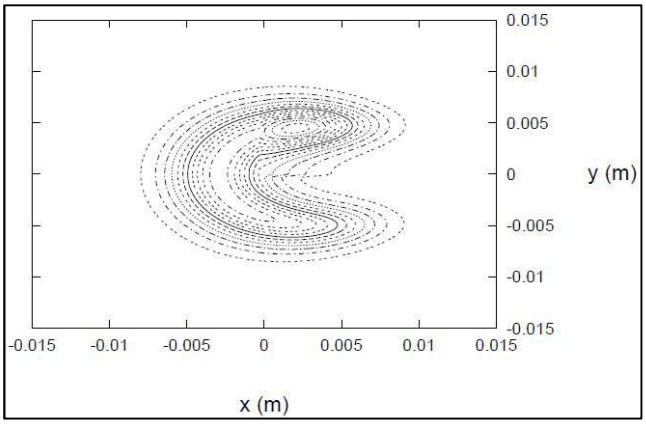

Figure 8. *Normalized intensity distribution of laser beam at z = 30 m with v = 0.05 m/s and 10% relative humidity. Intervals of contour lines are 0.1.*

As shown in Figures 6 and 7, at the outset of the thermal distortion effects, the laser beams are slightly contracted in the ± y direction and shifted into the direction of the flow.

When the thermal distortion becomes more severe, the self-induced thermal lens effect is clearly visible. As shown in Figure 8, the narrowing and/or focusing of the beam occurs along the flow direction and the peak intensity of the focalized beam exceeds that of the initially collimated laser beam.

Figure 9 shows the maximum values of the normalized intensity distribution and the shift Δx in the x direction of the peak positions as a function of z.

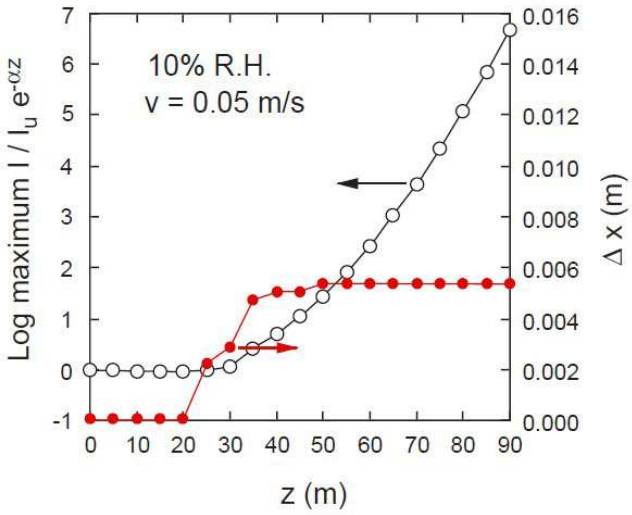

Figure 9. *The maximum values of the normalized intensity distribution and the shift Δ x in the x direction of the peak positions versus z with v = 0.05 m/s and 10% relative humidity.*

As shown in Figure 9, the maximum value increases rapidly with increasing z when $z \geq 30$ m. On the other hand, Δx increases with increasing z when $z \geq 25$ m and gradually reaches a constant value of 0.0053 m.

Figure 10 shows the normalized intensity distribution of laser beam at z = 65 m. In this figure, the intensity distribution is shown by contour lines with intervals of 100. As shown in this figure, the laser power is concentrated in two narrow areas, which are asymmetrical with respect to the y = 0 axis. And the centers of these areas are located at x ~0.0053 m and $y \sim \pm 0.0050$ m.

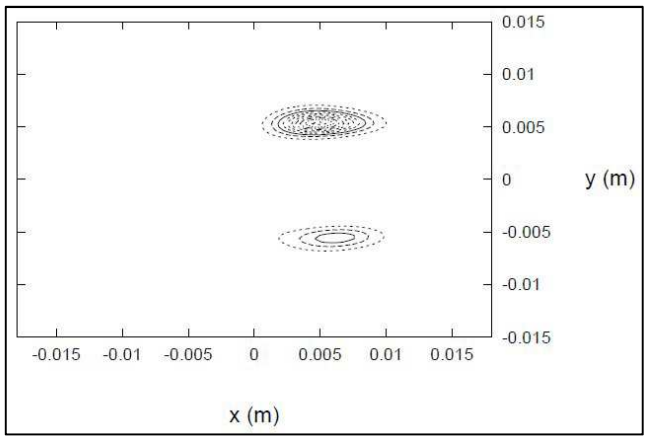

Figure 10. *Normalized intensity distribution of laser beam at z = 65 m with v = 0.05 m/s and 10% relative humidity. Intervals of contour lines are 100.*

To find the maximum shift value $\Delta^m x$ in the x direction, both sides of Eq. (10) were at first differentiated with respect to x. Then, assuming that the differentiated result was equal

to 0, we have the following equation:

$$4\left(\frac{x}{\omega}\right)^2 - 2 + \frac{\sqrt{\pi}}{2}\left(1 - 4\frac{y^2}{\omega^2}\right) = 0 \quad (12)$$

Using Eq. (12) and $y \simeq 0.0050$ m, $\Delta^m x$ is given by

$$\Delta^m x \cong 1.070 \cdot \omega = 0.0054\, m \quad (13)$$

This $\Delta^m x$ (0.0054 m) is close to the Δx (~0.0053 m) observed in Figure 10.

Thus, under conditions of v = 0.05 m/s (calm wind) and 10% relative humidity, laser beams can propagate only 25 to 30 m at most without damaging the initial beam shape, even in crosswinds.

Intensity distribution of laser beam is affected by wind velocity. In the next subsection, we describe high-power laser beam propagation under conditions of v = 0.5 m/s (light wind) at λ_0 = 1.08 μm.

3.3. Laser Beam Propagation with Light Uniform Wind

We investigated the intensity distributions of laser beam under the condition of light uniform wind (v = 0.5 m/s) when P = 1 kW, ω = 5 mm, 10% relative humidity, and λ_0 = 1.08 μm.

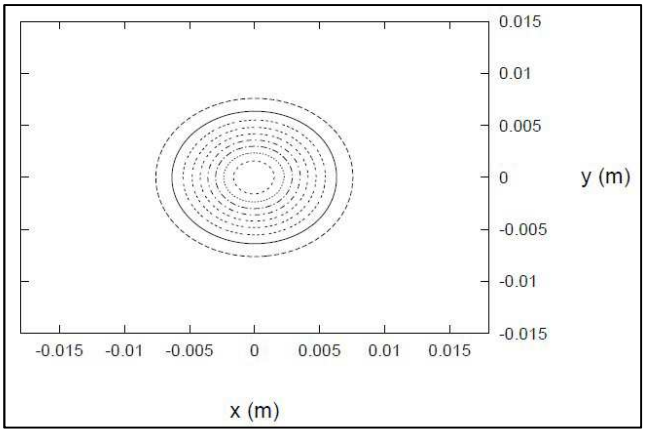

Figure 11. *Normalized intensity distribution of laser beam at z = 10 m with v = 0.5 m/s and 10% relative humidity. Intervals of contour lines are 0.1.*

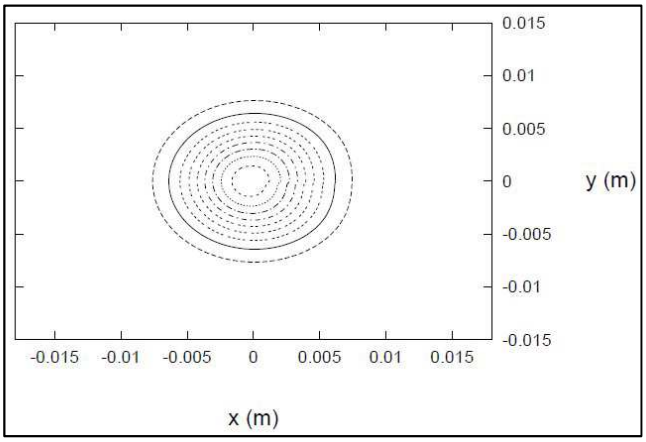

Figure 12. *Normalized intensity distribution of laser beam at z = 20 m with v = 0.5 m/s and 10% relative humidity. Intervals of contour lines are 0.1.*

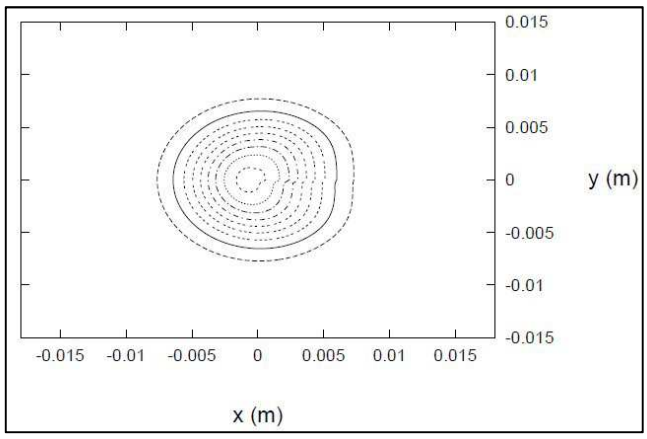

Figure 13. *Normalized intensity distribution of laser beam at z = 30 m with v = 0.5 m/s and 10% relative humidity. Intervals of contour lines are 0.1.*

The intensity distributions of laser beam at z = 10, 20, and 30 m were calculated using Eq. (10) when v = 0.5 m/s, 10% relative humidity, P = 1 kW, ω = 5 mm, and λ_0 = 1.08 μm. The calculated results are shown in Figures 11-13. In these figures, the normalized intensity distributions are shown by contour lines with intervals of 0.1.

As shown in Figures 11-13, the laser beams are slightly contracted in the ± y direction and shifted into the direction of the flow. However, even at z = 30 m, the self-induced thermal lens effect does not occur.

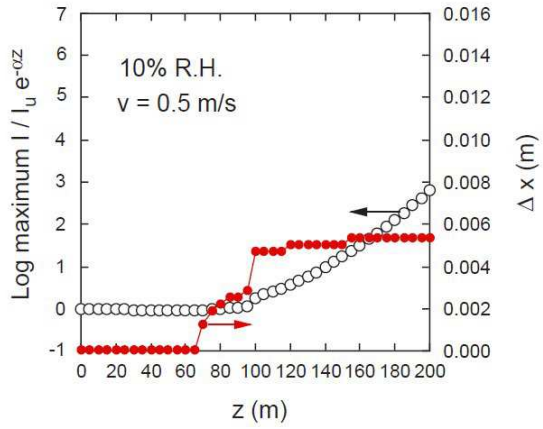

Figure 14. *The maximum values of the normalized intensity distribution and the shift Δ x in the x direction of the peak positions versus z with v = 0.5 m/s and 10% relative humidity.*

Figure 14 shows the maximum values of the normalized intensity distribution and the shift Δx in the x direction of the peak positions as a function of z.

As shown in Figure 14, the maximum value increases gradually with increasing z when $z \geq 100$ m. On the other hand, Δx increases with increasing z when $z \geq 70$ m and reaches a constant value of 0.0053 m.

Thus, under conditions of v = 0.5 m/s and 10% relative humidity, laser beams can propagate 65 to 70 m at most without damaging the initial beam shape. This distance (65-70 m) is double that (25-30 m) of the calm wind condition.

As described above, intensity distribution of laser beam is

affected by humidity and wind velocity, and the distance at which the initial beam shape can be maintained can be increased by increasing the wind speed.

4. Conclusion

In order to deliver high-power laser beam to a distant place, the laser beam must propagate through the atmosphere. When the laser beam propagates through a medium, a fraction of the laser energy is absorbed by the medium. This absorbed power heats the medium and alters the index of refraction of the path, and leads to a distortion of the beam itself. This phenomenon is called thermal blooming. Thermal blooming at $\lambda_0 = 1.08$ μm is caused by the absorption of water vapor. In this article, high-power laser beam propagation in a slightly wet atmosphere at $\lambda_0 = 1.08$ μm was theoretically investigated. At First, the absorption coefficient (α) of air at 10% relative humidity was estimated. Then, simulation of thermal blooming of Gaussian laser beam with an initial power of 1 kW and a radius of 5mm was conducted using this α. Under the condition of no wind, the beam intensity decreases rapidly with increasing length z. At $z = 16$ m, the intensity of laser beam became 1/5 of the initial intensity at $z = 0$ m. Under the condition of calm uniform wind with velocity (v) of 0.05 m/s, laser beams propagated only 25 to 30 m at most without damaging the initial beam shape. On the other hand, beams propagated 65 to 70 m at most without beam-shape deformation under the condition of light uniform wind with $v = 0.5$ m/s.

References

[1] Richardson D. J., Nilsson J., and Clarkson W. A. (2010). High power fiber lasers: current status and future perspectives. J. Opt. Soc. Am. B, 27 (11), B63-B92.

[2] Tünnermann A., Schreiber T., and Limpert J. (2010). Fibre lasers and amplifiers: an ultrafast performance evolution. Appl. Opt., 49 (25), F71-F78.

[3] Jauregui C., Limpert J., and Tünnermann A. (2013). High-power fibre lasers. Nat. Photonics, 7, 861-867.

[4] Fermann M. E. and Hartl I. (2013). Ultrafast fibre lasers. Nat. Photonics, 7, 868-874.

[5] Zervas M. N. and Codemand C. A. (2014). High power fiber lasers: a review. IEEE J. Selected Topics Quantum Electron., 20 (5), 0904123.

[6] Shi W., Fang Q., Zhu X., Norwood R. A., and Peyghambarian N. (2014). Fiber lasers and their applications. Appl. Opt., 53 (28), 6554-6568.

[7] Jeong Y., Sahu J. K., Williams R. B., Richardson D. J., Furusawa K., and Nilsson J. (2003). Ytterbium-doped large-core fibre laser with 272 W output power. Electron. Lett., 39 (13), 977-978.

[8] Limpert J., Liem A., Zellmer H., and Tünnerman A. (2003). 500 W continuous-wave fibre laser with excellent beam quality. Electron. Lett., 39 (8), 645-647.

[9] Liu C.-H., Ehlers B., Doerfel F., Heinemann S., Carter A., Tankala K., Farroni J., and Galvanauskas A. (2004). 810 W continuous-wave and single-transverse-mode fibre laser using 20 μm core Yb-doped double-clad fibre. Electron. Lett., 40 (23), 1471-1472.

[10] Jeong Y., Sahu J. K., Payne D. N., and Nilsson J. (2004). Ytterbium-doped large-core fibre laser with 1 kW of continuous-wave output power. Electron. Lett., 40 (8), 470-471.

[11] Jeong Y., Sahu J. K., Payne D. N., and Nilsson J. (2004). Ytterbium-doped large-core fiber laser with 1.36 kW continuous-wave output power. Opt. Express, 12 (25), 6088-6092.

[12] He B., Zhou J., Lou Q., Xue Y., Li Z., Wang W., Dong J., Wei Y., and Chen W. (2010). 1.75-kilowatt continuous-wave output fiber laser using homemade ytterbium-doped large-core fiber. Microwave Opt. Technol. Lett., 52 (7), 1668-1671.

[13] Jeong Y., Boyland A. J., Sahu J. K., Chung S., Nilsson J., and Payne D. N. (2009). Multi-kilowatt single-mode ytterbium-doped large-core fiber laser. J. Opt. Soc. Korea, 13 (4), 416-422.

[14] Huang L., Wang W., Leng J., Guo S., Xu X., and Cheng X. (2014). Experimental investigation on evolution of the beam quality in a 2-kW high power fiber amplifier. IEEE Photon. Technol. Lett., 26 (1), 33-36.

[15] Khitrov V., Minelly J. D., Tumminelli R., Petit V., and Pooler E. S. (2014). 3 kW single-mode direct diode-pumped fiber laser. Proc. Soc. Photo-Opt. Instrum. Eng., 8961, 89610V-1-89610V-6.

[16] Yu H., Zhang H., Lv H., Wang X., Leng J., Xiao H., Guo S., Zhou P., Xu X., and Chen J. (2015). 3.15 kW direct diode-pumped near diffraction-limited all-fiber-integrated fiber laser. Appl. Opt., 54 (14), 4556-4560.

[17] Rosales-Garcia A., Tobioka H., Abedin K., Dong H., Várallyay Z., Szabo A., Taunay T., Sullivan S., and Headley C. (2015). 2.1 kW single mode continuous wave monolithic fiber laser. Proc. Soc. Photo-Opt. Instrum. Eng., 9344, 93441G-1-93441G-6.

[18] Beier F., Hupel C., Nold J., Kuhn S., Hein S., Ihring J., Sattler B., Haarlammert N., Schreiber T., Eberhardt R., and Tünnermann A. (2016). Narrow linewidth, single mode 3 kW average power from a directly diode pumped ytterbium-doped low NA fiber amplifier. Opt. Express, 24 (6), 6011-6020.

[19] Mashiko Y., Nguyen H. K., Kashiwagi M., Kitabayashi T., Shima K., and Tanaka D. (2016). 2 kW single-mode fiber laser with 20-m long delivery fiber and high SRS suppression. Proc. Soc. Photo-Opt. Instrum. Eng., 9728, 972805-1-972805-6.

[20] Beier F., Hupel C., Kuhn S., Hein S., Nold J., Proske F., Sattler B., Liem A., Jauregui C., Limpert J., Haarlammert N., Schreiber T., Eberhardt R., and Tünnermann A. (2017). Single mode 4.3 kW output power from a diode-pumped Yb-doped fiber amplifier. Opt. Express, 25 (13), 14892-14899.

[21] Ikoma S., Nguyen H. K., Kashiwagi M., Uchiyama K., Shima K., and Tanaka D. (2017). 3 kW single stage all-fiber Yb-doped single-mode fiber laser for highly reflective and highly thermal conductive material processing. Proc. Soc. Photo-Opt. Instrum. Eng., 10083, 100830Y-1-100830Y-6.

[22] Su R., Tao R., Wang X., Zhang H., Ma P., Zhao P., and Xu X. (2017). 3.7 kW monolithic narrow linewidth single mode fiber laser through simultaneously suppressing nonlinear effects and mode instability. Laser Phys. Lett., 14, 085102.

[23] Wang Y., Gao C., Tang X., Zhan H., Peng K., Ni L., Liu S., Li Y., Guo C., Wang X., Zhang L., Yu J., Jiang L., Lin H., Wang J., Jing F., and Lin A. (2018). 30/900 Yb-doped aluminophosphosilicate fiber presenting 6.85-kW laser output pumped with commercial 976-nm laser diodes. IEEE J. Lightwave Technol., 36 (16), 3396-3402.

[24] Xiao Q., Li D., Huang Y., Wang X., Wang Z., Tian J., Yan P., and Gong M. (2018). Directly diode and bi-directional pumping 6 kW continuous-wave all-fibre laser. Laser Phys., 28, 125107.

[25] Shima K., Ikoma S., Uchiyama K., Takubo Y., Kashiwagi M., and Tanaka D. (2018). 5-kW single stage all-fiber Yb-doped single-mode fiber laser for material processing. Proc. Soc. Photo-Opt. Instrum. Eng., 10512, 105120C-1-105120C-6.

[26] Lin H., Tao R., Li C., Wang B., Guo C., Shu Q., Zhao P., Xu L., Wang J., Jing F., and Chu Q. (2019). 3.7 kW monolithic narrow linewidth single mode fiber laser through simultaneously suppressing nonlinear effects and mode instability. Opt. Express, 27 (7), 9716-9724.

[27] Lin H., Xu L., Li C., Shu Q., Chu Q., Xie L., Guo C., Zhao P., Li Z., Wang J., Jing F., and Tang X. (2019). 10.6 kW high-brightness cascade-end-pumped monolithic fiber lasers directly pumped by laser diodes in step-index large mode area double cladding fiber. Results in Phys., 14, 102479.

[28] Ye Y., Yang B., Shi C., Xi X., Zhang H., Wang X., Zhou P., and Xu X. (2020). Towards power improvement of all-fiber laser oscillators with 30 μm-core Yb-doped fibers by suppressing transverse mode instability. Laser Phys. Lett., 17, 085106.

[29] Ye Y., Yang B., Wang P., Zeng L., Xi X., Shi C., Zhang H., Wang X., Zhou P., and Xu X. (2021). Industrial 6 kW high-stability single-stage all-fiber laser oscillator based on conventional large mode area ytterbium-doped fiber. Laser Phys., 31, 035104.

[30] Stachowiak D. (2018). High-power passive fiber components for all-fiber lasers and amplifiers application-design and fabrication. Photonics, 5, 38-1-38-17.

[31] Beaudou B., Gerôme F., Wang Y. Y., Alharbi M., Bradley T. D., Humbert G., Auguste J.-L., Blondy J.-M., and Benabid F. (2012). Millijoule laser pulse delivery for spark ignition through kagome hollow-core fiber. Opt. Lett., 37 (9), 1430-1432.

[32] Jaworski P., Yu F., Maier R. R. J., Wadsworth W. J., Knight J. C., Shephard J. D., and Hand D. P. J. (2013). Picosecond and nanosecond pulse delivery through a hollow-core negative curvature fiber for micro-machining applications. Opt. Express, 21 (19), 22742-22753.

[33] Ulrich A., Maier R. R. J., Yu F., Knight J. C., Hand D. P. J., and Shephard J. D. (2013). Flexible delivery of Er:YAG radiation at 2.94 μm with negative curvature silica glass fibers: a new solution for minimally invasive surgical procedures. Biomedical Opt. Express, 4 (2), 193-205.

[34] Dumitrache C., Rath J., and Yalin A. P. (2014). High power spark delivery system using hollow core kagome lattice fibers. Materials, 7, 5700-5710.

[35] Michieletto M., Lyngso J. K., Jakobsen C., Laegsgaard J., Bang O., and Alkeskjold T. T. (2016). Hollow-core fibers for high power pulse delivery. Opt. Express, 24 (7), 7103-7119.

[36] Elizer S. and Wedel B. (2018). Hollow core optical fibers for industrial ultra short pulse laser beam delivery applications. Fibers, 6, 80-1-80-11.

[37] Matsui T, Tsujikawa K, Okuda T., Hanzawa N., Sagae Y., Nakajima K., Fujiya Y., and Shiraki K. (2020). Effective area enlarged photonic crystal fiber with quasi-uniform air-hole structure for high power transmission. IEICE Trans. Commun., E103-B (4), 415-421.

[38] Zhu X., Wu D., Wang Y., Yu F., Li Q., Qi Y., Knight J., Chen S., and Hu L. (2021). Delivery of CW laser power up to 300 Watts at 1080 nm by an uncooled low-loss ant-resonant hollow-core fiber. Opt. Express, 29 (2), 1492-1501.

[39] Smith D. C. (1977). High-power laser propagation: thermal blooming. Proc. IEEE, 65 (12), 1969-1714.

[40] Gebhardt F. G. and Smith D. C. (1969). Effects of wind on thermal defocusing of CO_2 laser radiation. Appl. Phys. Lett., 14 (2), 52-54.

[41] Smith D. C. (1969). Thermal defocusing of CO_2 laser radiation in gases. IEEE J. Quantum Electron., QE-5 (12), 600-607.

[42] Smith D. C. and Gebhardt F. G. (1970). Saturation of the self-induced thermal distortion of laser radiation in a wind. Appl. Phys. Lett., 16 (7), 275-278.

[43] Kenemuth J. R., Hogge C. B., and Avizonis P. V. (1970). Thermal blooming of a 10.6-μ laser beam in CO_2. Appl. Phys. Lett., 17 (5), 220-223.

[44] Wallace J. and Camac M. (1970). Effects of absorption at 10.6 μ on laser-beam transmission. J. Opt. Soc. Am., 60 (12), 1587-1594.

[45] Gebhardt F. G. and Smith D. C. (1971). Self-induced thermal distortion in the near field for a laser beam in a moving medium. IEEE J. Quantum Electron., QE-7 (2), 63-73.

[46] Gebhardt F. G. and Smith D. C. (1972). Effects of diffraction of the self-induced thermal distortion of a laser beam in a crosswind. Appl. Opt., 11 (2), 244-248.

[47] Avizonis P. V., Hogge C. B., Butts R. R., and Kenemuth J. R. (1972). Geometric optics of thermal blooming in gases. Part 1. Appl. Opt., 11 (3), 554-564.

[48] Hayes J. N., Ulrich P. B., and Aitken A. H. (1972). Effects of the atmosphere on the propagation of 10.6-μ laser beams. Appl. Opt., 11 (2), 257-260.

[49] Wallace J. (1972). Effects of nonlinear refraction at 10.6 μm on the far-field irradiance distribution. J. Opt. Soc. Am., 62 (3), 373-378.

[50] Aitken A. H., Hayes J. N., and Ulrich P. B. (1973). Thermal blooming of pulsed focused Gaussian laser beams. Appl. Opt., 12 (2), 193-197.

[51] Ulrich P. B. and Wallace J. (1973). Propagation characteristics of collimated pulsed laser beams through an absorbing atmosphere. J. Opt. Soc. Am., 63 (1), 8-12.

[52] Fleck, Jr. J. A., Morris J. R., and Feit M. D. (1976). Time-dependent propagation of high energy laser beams through atmosphere. Appl. Phys., 10, 129-160.

[53] Fleck, Jr. J. A., Morris J. R., and Feit M. D. (1976). Time-dependent propagation of high energy laser beams through atmosphere: II. Appl. Phys., 14, 99-115.

[54] Sprangle P., Ting A., Peňano J., Fischer R., and Hafizi B. (2009). Incoherent combining and atmospheric propagation of high-power fiber lasers for directed-energy applications. IEEE J. Quantum Electron., 45 (2), 138-148.

[55] Sprangle P., Hafizi B., Ting A., and Fischer R. (2015). High-power lasers for directed-energy applications. Appl. Opt., 54 (31), F201-F209.

[56] Curcio J. A. and Petty C. C. (1951). The near infrared absorption spectrum of liquid water. J. Opt. Soc. Am., 41 (5), 302-304.

[57] Tetens O. (1930). Uber einige meteorologische begriffe. Z. Geophys., 6, 297-309.

[58] Shoji M. (1995). Heat Transfer Textbook. Appendix F, University of Tokyo Press, Tokyo.

[59] Chemical Society of Japan. (1984). Chemical Data Book. 3rd Ed., Chap. 5, Maruzen, Tokyo.